

Article

A Study of Magnetic Mill Productivity

Dariusz Całus ^{1,*} , Oleksandr Makarchuk ^{1,2} , Piotr Domanowski ³  and Sławomir Bujnowski ³

¹ Faculty of Electrical Engineering, Czestochowa University of Technology, 42-201 Czestochowa, Poland; oleksandr.makarchuk@pcz.pl

² Institute of Power Engineering and Control Systems, Lviv Polytechnic National University, 79013 Lviv, Ukraine

³ Faculty of Mechanical Engineering, Bydgoszcz University of Science and Technology, 7 Kaliskiego Ave., 85-796 Bydgoszcz, Poland; piotr.domanowski@pbs.edu.pl (P.D.); slawomir.bujnowski@pbs.edu.pl (S.B.)

* Correspondence: dariusz.calus@pcz.pl

Abstract: The paper explores the characteristic indicators of the operation of a magnetic mill. A magnetic mill is a device designed for grinding or mixing substances by interaction with ferromagnetic working elements moving in a rotating magnetic field. The study established the main factors influencing force interaction between the components of such a system. An analysis of the magnetic field inside the working zone of the mill was conducted and the method of calculating the quantitative indicators of this interaction was found. The method responds to changes in the size of these elements, their position in the mill working area and changes in the intensity of the magnetic field. A mathematical model was developed. The model is used for calculating the trajectories of movement of the ferromagnetic elements that are placed in a rotating magnetic field and are confined by space of the working zone of the mill. Indicators directly related to the productivity of the grinding/mixing process were determined following an analysis of the simulation results. Based on comparison of the results obtained by calculation and experimental methods, it was proven that the proposed method is suitable for evaluating the productivity of the grinding/mixing process in a real technological system containing a magnetic mill.

Keywords: magnetic mill; productivity; grinding; mixing; rotating magnetic field inductor; FEM analysis



Citation: Całus, D.; Makarchuk, O.; Domanowski, P.; Bujnowski, S. A Study of Magnetic Mill Productivity. *Appl. Sci.* **2023**, *13*, 6538. <https://doi.org/10.3390/app13116538>

Academic Editor: Edik U. Rafailov

Received: 8 May 2023

Revised: 24 May 2023

Accepted: 25 May 2023

Published: 27 May 2023



Copyright: © 2023 by the authors. Licensee MDPI, Basel, Switzerland. This article is an open access article distributed under the terms and conditions of the Creative Commons Attribution (CC BY) license (<https://creativecommons.org/licenses/by/4.0/>).

1. Introduction

Technological devices intended for grinding or mixing various mixtures (including aggressive ones, for example, based on acids or alkalines) are an integral part of many technological processes used in modern industrial production. Examples of such equipment are magnetic (MM) or electromagnetic (EMM) mills. The technological process in these mills takes place inside a working chamber (WC), due to force interaction (impacts, collisions, friction, vibrations, etc.) of the working elements with the substance intended for grinding or mixing. This substance is hereinafter referred to as the working substance (WS), and the working elements are hereinafter referred to as millstones.

Electromagnetic methods of intensification of technological processes, that is, methods in which energy of an electromagnetic field plays the role of an effective factor, are used by many industrial sectors. In particular, these include the processing and enrichment of fossil fuels, reducing the production of harmful compounds and minimizing their release into the environment, reducing the amount of waste, using secondary raw materials and introducing the latest energy-saving technologies, etc. Therefore, studies in this direction can be considered a search for ways to solve the global complex problem of environmental protection.

2. Analysis of the Latest Studies

Modern publications present a fairly wide range of studies on industrial mills, whose principle of operation is based on moving ferromagnetic millstones in a magnetic field. Two competing technologies are mainly considered. One of them is based on creating a rotating magnetic field using a fixed inductor containing a multiphase symmetrical winding connected to a multiphase alternating current network (most often three-phase) [1–3]. The second technology is much less frequently used. Its application involves the creation of a magnetic field with the help of permanent magnets located on a rotating inductor [4].

Several directions of research into such mills are distinguished, particularly the following:

- the development of inductor structures and working out design calculation methods [1,5,6];
- establishing interrelationships between the structural parameters of the mill and the course of the characteristic physical processes in its WC [2–4,7–16];
- the creation and improvement of management systems [3,6,17–22];
- experimental studies of grinding and/or mixing processes [1,2,5,14,19,23–25];
- the improvement of existing and development of new technological processes that involve mills [5,11,20,22,26–29].

A review of publications on the issue under study proves its relevance and highlights existing problems. For instance, [1] emphasizes the advantages of using EMMs compared to traditional ball mills as exemplified by the process of grinding copper ore.

The obvious advantages of the electromagnetic method of creating a rotating field, namely the energy of the field being directly transmitted to the ferromagnetic millstones, prompted the authors of [1,3,6] to use it for construction of an EMM prototype. However, this approach has particular drawbacks. The inductor of such a mill consumes reactive current from the network; consequently, it will require a compensating device to maintain the power factor within acceptable limits. It is also expedient for this device to be adjustable. The phase shift angle between voltage and current will depend on the number of millstones in the WC, their size and location. In addition, in order to achieve significant values of magnetic induction in the WC and to reduce the dispersion of the magnetic field in such an inductor, its main dimensions (diameter, length) should be as small as possible. This implies using rather complex cooling systems for such inductors.

In [3,8,18,25] the authors take into account effects of the electromagnetic mill control system together with its cooling system, WS flow regulator, filters and separators, various purification systems, heat exchanger and WS flow recirculation system for supplementary grinding. Based on the results of the mathematical modeling of processes in such a technological complex, conclusions about efficiency of the mill are presented. A real-time control system for the energy efficiency of this mill is proposed in [19]. Moreover, the aforementioned set of equipment is used for conducting experimental studies [2,25].

In [27], an innovative coal grinding technology for increasing the efficiency of fuel boilers is considered. This scientific paper discusses the importance of achieving the appropriate level of fuel granularity, which directly affects this indicator. Similar problems are considered in [25]. The authors study experimental results of the dry and wet grinding method, establishing the size distribution of the obtained particles, which provides an objective assessment of productivity of the technologies used.

The authors of [20,25] claim that a complex of factors acting on the substance placed in the working chamber of the magnetic mill can lead to deformation of the crystal lattice of a solid substance, a sharp increase in its chemical activity, degree of dissociation, etc. These factors are mechanical collisions of particles of the substance with millstones and resulting local centers of high temperature and pressure, sound and ultrasonic vibrations, cavitation and electrolysis phenomena that occur as a result of the movement of ferromagnetic elements, as well as the rotating magnetic field. This will create conditions for such physicochemical processes that are impossible or complicated under normal conditions. Increasing the chemical activity of solid particles by grinding them is called the activation

of a substance. Activation using a magnetic field allows the intensification of various technological processes and the increase in their energy efficiency [26].

In [9,18], the authors try to mathematically formalize a description of the processes of the mechanical processing of materials using genetic algorithms and neural networks. The link between the design parameters of the working elements and performance of the process is presented in a declarative form; the direct influence of these parameters on the processing workflow is not shown.

Many publications are devoted to experimental studies of both grinding processes and the aforementioned equipment [1,20,24,29]. Such works make it possible, to a certain extent, to verify the theoretical approaches used to evaluate and analyze the grinding process as a separate phenomenon, as well as energy exchange processes in mills that are part of certain technological lines.

Problems of grinding quality control are considered in [11,17,22,25,28,29]. Refs. [15,24] proposes implementation of constant monitoring of the temperature of the grinding process.

In the present study, a mill is considered wherein the magnetic field is created by permanent magnets (PM). However, the developed method of analyzing the dynamic interaction of millstones in the WC of such a mill can be relatively easily adapted for EMMs in which the magnetic field is created by a multiphase system of alternating currents [12–14].

3. Problem Statement

The productivity of a mill performing the functions of grinding the working substance with the help of a magnetic field is determined by efficiency of conversion of the energy consumed into energy spent on comminuting this substance. The transmission mechanism and stages of energy conversion, as well as the type and intensity of dynamic interactions of the substance with the millstones, depend on the design of this equipment and the method of forming the dispersive force. Therefore, in order to theoretically assess the productivity of the MM, it is necessary to establish a deterministic interrelationship between the design parameters of the mill (dimensions, magnetic properties of materials, etc.) and the quantitative indicators of the above-mentioned effort.

The analysis of publications showed that theoretical research methods have particular shortcomings, namely:

- existing MM project design methods either do not relate structural parameters to the performance of the grinding/mixing process at all or do it using empirical dependencies obtained by processing experimental data and for a rather narrow range of variations of structural parameters;
- optimization methods of technological process control systems using MM are based on the results of mathematical modeling that consists of statistical processing of experimental data;
- insufficient attention is paid to developing online methods for evaluating the quality of grinding products directly during processing or immediately after it.

Among the design flaws inherent in EMMs, the following ones can be noted:

- salient-pole EMM inductors are characterized by an increased level of magnetic field dispersion, at the level of 20–40%, which negatively affects the efficiency of the energy conversion process as a whole;
- the EMM inductor works with a low power factor; consequently, it requires the use of compensating devices.

The purpose of the research is to identify indicators directly affecting the productivity of the grinding/mixing process; to develop a method of quantitative assessment of these indicators depending on the size of the mill working chamber, the number and size of the millstones and parameters of the inductor.

The object of the research is the processes of dynamic interaction between ferromagnetic mills, the substance being ground/mixed and the working chamber, in the rotating magnetic field inside this chamber.

4. Description of the Construction and Principle of Operation

The mill chosen by us for the study consists of a magnetic field inductor 1 rotating around a working chamber 2, an electric engine 3, a supporting and rotating device 4 and a bed plate 5 (Figure 1). The inductor is a hollow steel cylinder, with permanent magnet poles on the inner surface. Powered by a drive motor, the inductor rotates around the WC and creates a rotating magnetic field inside it. It interacts with ferromagnetic millstones 6 located inside the WC and sets them in motion. In turn, this affects the WS with impact and abrasion loads.

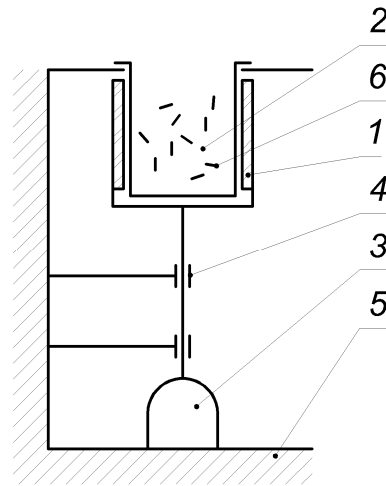


Figure 1. Kinematic scheme of the magnetic mill: 1—inductor with permanent magnets; 2—working chamber with millstones; 3—driving engine; 4—supporting and rotating device; 5—bed plate; 6—millstone.

The proposed construction scheme of a mill with an inductor containing PM is characterized by certain advantages compared to mills with electromagnetic field excitation. In particular, the manufacturing technology is relatively simple. It is possible to change the topology of the magnetic field in the WC, achieving greater productivity of the grinding/mixing process. There is no system for the forced cooling of the inductor; there is no need for devices that would compensate for consumed reactive power. This makes it possible to consider such a mill design to be competitive. It is also obvious that this device is not without its drawbacks: it needs a driving engine and there are limitations on the achievable level of magnetic induction in the WC.

5. Research Methods

Study of the dynamic behavior of ferromagnetic millstones in the rotating magnetic field of the inductor was based on the calculation of the field of ponderomotive forces in two-dimensional quasi-stationary approximation acting on these millstones in the middle of the WC. The calculation of these forces was conducted using the so-called Maxwell tension tensor [30]. At the same time, it was considered that the force acting on any part of volume V , limited by surface S , can be obtained by summing elementary forces $d\vec{F} = \vec{F}_n d\vec{S}$, attached to elements $d\vec{S}$ surface S , respectively:

$$\vec{F} = \int_S \vec{F}_n d\vec{S}, \quad (1)$$

where \vec{F}_n —is the tension force acting from the outside on the elementary surface, the external standard part to which is directed along \vec{n}

$$\vec{F}_n = \lim_{\Delta S \rightarrow 0} \frac{\Delta \vec{F}}{\Delta S}. \quad (2)$$

In a two-dimensional formulation, the vector of the resulting force is calculated as

$$\bar{F} = \frac{1}{\mu_0} \oint_l \mathbf{T}_m \bar{n} d\bar{l}, \tag{3}$$

where $\mathbf{T}_m = \begin{vmatrix} \frac{1}{2}(B_x^2 - B_y^2) & B_x B_y \\ B_x B_y & \frac{1}{2}(-B_x^2 + B_y^2) \end{vmatrix}$ —is the Maxwell tension tensor for an isotropic medium; B_x, B_y are projections of the magnetic induction vector to the outside of the surface S ; and \bar{n} is the standard part of this surface.

To determine the electromagnetic moment rotating a separate millstone relative to the axis passing through its center of mass, the above approach was also used (3). After particular transformations of this expression, the moment was determined as

$$M_0 = \bar{z} \cdot \frac{1}{\mu_0} \int_l \bar{r} \times \left[(\bar{n} \cdot \bar{B}) \cdot \bar{B} - \frac{1}{2}(\bar{B} \cdot \bar{B}) \cdot \bar{n} \right] d\bar{l}, \tag{4}$$

where \bar{z} is a unit vector directed along the axis of rotation; \bar{r} is the radius vector, the end of which belongs to the outer contour of the millstone.

6. Indicators of Force Interaction of Millstones in a Rotating Magnetic Field

In order to find out the factors affecting the force interaction of millstones with each other, with the WS and with the walls of the WC, an analysis of the magnetic field inside the WC was conducted, and a mathematical model was created to calculate the quantitative indicators of this interaction. It has been established that the forces of magnetic origin acting on a separate millstone depend on its position in the WC, the intensity of the magnetic field, the material from which the millstone is made, the level of the filling of the WC with millstones, etc.

Let us attach a fixed polar coordinate system to an arbitrary cross-section of the working chamber that allows setting the coordinates of the position of the center of mill mass using the length of the radius vector r_m and the angle of its inclination γ_m to the axis $+r$ (Figure 2). The position of the millstone will set the angle of inclination of its longitudinal axis α_m to the direction of the radius vector. Hereinafter, cylindrical millstones were considered, the dimensions of which were designated as d_m and l_m .

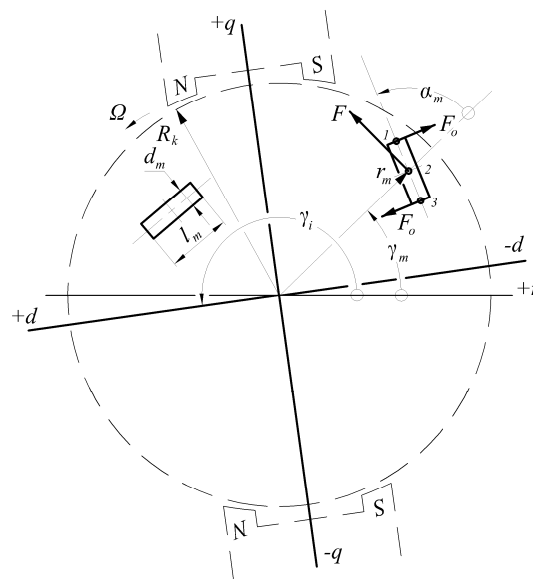


Figure 2. The coordinate system of the model and a schematic of force application.

A number of mathematical experiments were conducted to establish the functional interrelationships between forces, moments and the aforementioned indicators. The inductor with PM was selected; the volume of the WC was 300 cm³. The main dimensions of the mill are as follows: the calculated length is 80 mm; the diameter of the WC is 120 mm. The pole tips of the inductor are made of electrotechnical steel M600-50A; permanent magnets of the N38 brand are made of rare earth powder material based on neodymium, iron and boron (residual induction 1.2 T, coercive force 800 kA/m), and the millstone is made of carbon steel A283/C. The average turnover value of the magnetic induction in the WC is 0.052 T. The sizes of the millstones used in the experiment were $d_m = 1.5$ mm and $l_m = 12$ mm. The shape of the cross-section and the level of discretization of the computational domain are shown in Figure 3.

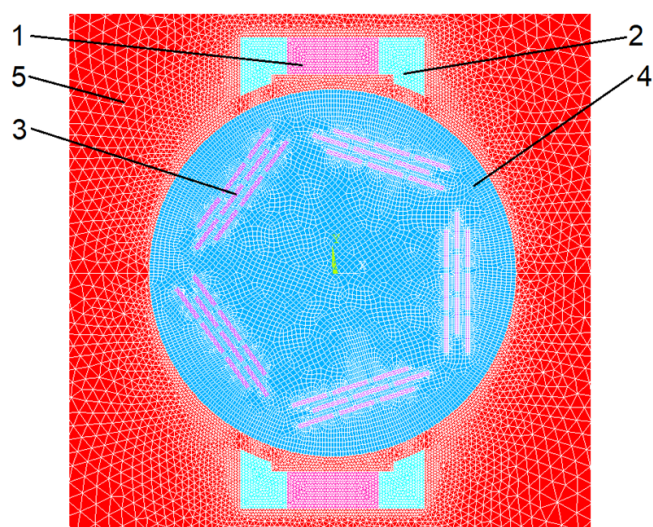


Figure 3. Fragment of the calculation area of the FEM model of MM: 1—pole with PM; 2—pole tips; 3—millstones; 4—working chamber; 5—environment.

The dependencies of the force applied to the center of millstone mass and the torque acting on a separate millstone relative to the coordinates determining its position inside the working chamber (r_m, γ_m), the angle of rotation of the millstone α_m and as the angle of rotation of axis $\gamma_i + d$ of the magnetic system of the inductor were determined. To reduce the number of scalar arguments, the relative location of the angular position of the center of the millstone and the axis $+d$ was determined by the difference

$$\gamma = \gamma_i - \gamma_m. \tag{5}$$

We shall hereinafter refer to the angle γ as the angular displacement between the inductor and a millstone or, in short, the angular displacement.

It is obvious that in real conditions each millstone is surrounded by others, which, in turn, affects the distribution of the magnetic field, the magnitude and direction of the force \bar{F}_m . To a certain extent, we have taken this influence into account by placing ‘surroundings’ of 8 similar millstones located around the millstone under study. In our opinion, this will increase the adequacy of the obtained results [12].

Figure 4 shows the vector diagram of the force \bar{F}_m depending on the angular position of the mill relative to the axis $+d$, which at the qualitative level clearly demonstrates the adequacy of the obtained results.

On the basis of the results obtained using the above-mentioned model, force hodographs \bar{F}_m , corresponding to a full rotation of the inductor, were constructed (Figure 5). It should be noted that the three dependencies shown in Figure 5a refer to various conditions for conducting a mathematical experiment. One of them corresponds to the location of a single fixed millstone in the WC, the second one to the location of an ordered set (domain) of

9 identical millstones, and the third one to the location of 5 such sets of 9 millstones. It is the last condition that corresponds to the image in Figure 3.

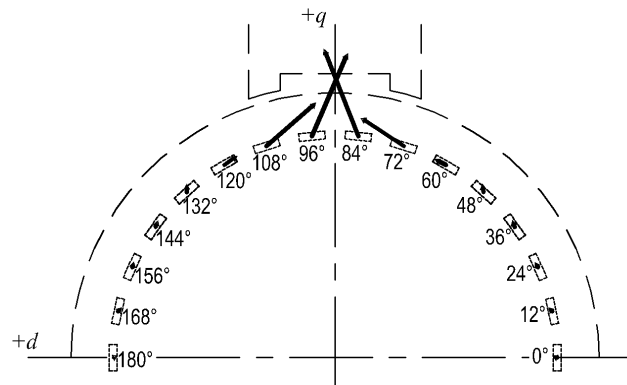


Figure 4. Vector diagram of forces acting on millstones in the WC.

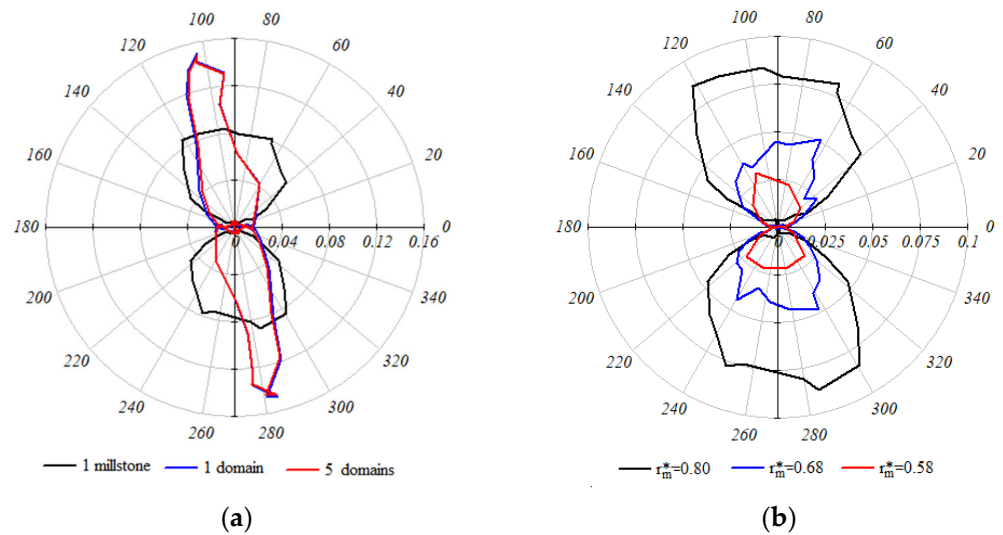


Figure 5. Hodographs of the vector \bar{F}_m , [N] depending on: (a) presence of ‘surroundings’ and $r_m^* = 0, 8$; (b) coordinates r_m^* for one millstone.

Figure 5a shows that the presence of the ‘surroundings’ has a rather strong effect on the magnitude of the force \bar{F}_m and practically does not affect its direction. The periodic nature of these dependencies with a period proportional to the number of poles of the magnetic system of the inductor is also obvious. This will be taken into account in further use of the given dependencies for an analytical description of the force field \bar{F}_m .

Analysis of the dependencies presented in Figure 5b gives grounds to assert that the magnitude of the vector \bar{F}_m does not depend linearly on the radial coordinate of the center of millstone mass; on the other hand, it practically does not affect the change in the direction of the force vector. Let us note that $r_m^* = r_m / R_k$ is the relative value of the radial coordinate of the mill center.

Figure 6 shows the dependence of the torque M_m relative to the axis passing through the center of mass of an individual millstone on the angular displacement γ . The periodic nature of these dependencies and the relatively weak nonlinear influence of the radial coordinate of location of the millstone on the value M_m are obvious.

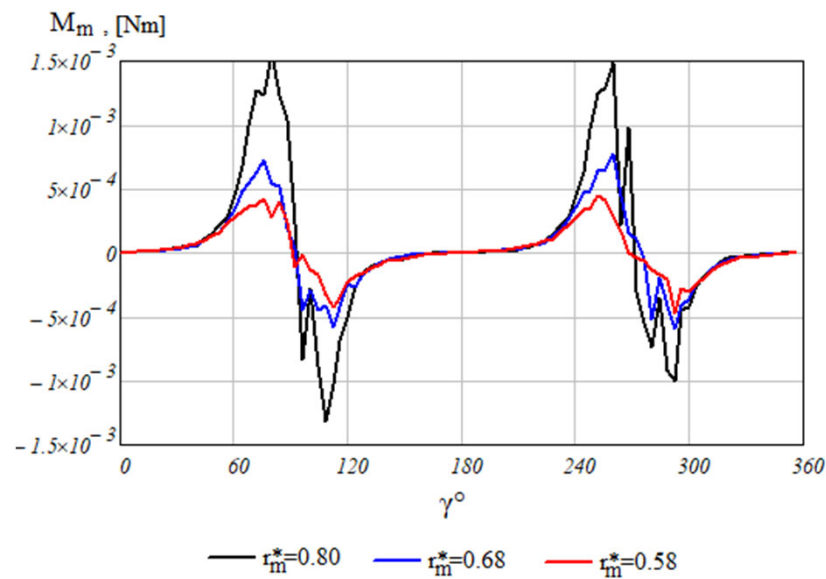


Figure 6. Dependencies of the torque M_m on the angle of rotation of the inductor.

The nature of dependencies $\bar{F}_m(\gamma, r_m)$ and $M_m(\gamma, r_m)$ is generally non-linear. This is explained by the non-linear links between magnetic field induction and forces of electromagnetic origin, as well as non-linear features of magnetization of ferromagnetic millstones and pole tips of the inductor. It can be argued that the analytical methods of representing these dependencies for the purpose of further use in solving problems of the dynamics of millstone movement in a rotating magnetic field are not implemented. Therefore, in our opinion, applying methods of invariant approximation theory of functions and interpolation theory is fully justified.

As a rule, all components of the raw materials to be ground are fed to the WC with the help of a stream of compressed air or liquid. Such a flow is also called a transport flow [3,8,18]. Consequently, another factor definitely affecting the course of the process of millstones interacting with WS particles is hydrodynamic resistance forces.

The inclusion of the influence of such a force was subsequently carried out without using the mathematical apparatus of the interpolation theory. In the case of the turbulent nature of the fluid motion ($Re > 10^4$), the value of the hydro resistance force is determined by using a Formula (6) developed on the basis of the known linear velocity of fluid streams or particles.

$$F_c = C_x S \frac{\rho v^2}{2}, \tag{6}$$

where C_x is the coefficient of frontal resistance (for a sphere it is 1.12);

S is the area of projection of a body onto a plane perpendicular to the trajectory of movement of this body; and

v is projection of the speed of a body movement in a still flow.

7. Development of Interpolation Algorithm

The accuracy of the approximation of the field of forces and moments acting on the millstone in the rotating magnetic field of the mill inductor will obviously determine the adequacy level of the entire model, which will describe the dynamic behavior of the millstones in the WC. Let us consider the basic approaches involved in the algorithm of interpolation of the field of forces and moments.

Using the results of modeling (Section 6), tabulated functions (TF) were obtained, which describe the field of forces \bar{F}_m and torque M_m , acting on the millstone, depending on a number of specific arguments, in particular, the position of the millstone in the WC, its orientation in it, etc. After analyzing the obtained results, we have left only 2 such

arguments, namely, the angular displacement of the inductor and the millstone γ and the radius of the center of the millstone mass r_m . These scalar TFs of the vector argument are combined into one vector function of the vector argument. For this purpose, the notation as below is introduced

$$\vec{S}_m = \begin{pmatrix} F_m \\ \alpha_m \\ M_m \end{pmatrix}; \quad \vec{z} = \begin{pmatrix} \gamma \\ r_m \end{pmatrix} \tag{7}$$

where F_m and α_m are the modulus and angle of inclination of the electrodynamic force vector \vec{F}_m in the Cartesian rectangular coordinate system, the origin of which coincides with the longitudinal axis of symmetry of the WC; M_m is torque relative to the center of millstone mass; γ is the mutual angular displacement, according to (5); and r_m is the length of the radius vector that determines the position of the millstone (Figure 2).

Therefore, the TF $\vec{S}_m(\vec{z})$ at the level of assumptions adopted by us describes the force effect of the magnetic field of the rotating inductor of MM on the ferromagnetic millstones located in the middle of its working chamber, taking into account their dimensions and the shape of the cross section, the size and shape of the WC, parameters and real topology of the magnetic field, including the configuration of the magnetic field of the inductor and its saturation.

We assumed that each of the components of the vector \vec{S}_m is approximated by a Taylor polynomial of the second degree with two independent variables γ and r_m . Then, the force modulus F_m can be represented as

$$F_m[\gamma, r_m] = c_1 + c_2\gamma + c_3r_m + c_3\frac{\gamma^2}{2!} + c_5\gamma r_m + c_6\frac{r_m^2}{2!} = \vec{T}[\gamma, r_m] \vec{c}, \tag{8}$$

where

$$\vec{T}[\gamma, r_m] = \begin{pmatrix} 1 & \gamma & r_m & \frac{\gamma^2}{2!} & \gamma \cdot r_m & \frac{r_m^2}{2!} \end{pmatrix}, \tag{9}$$

is Taylor’s series of the 2nd degree with two independent variables;

$$\vec{c} = \|c_1 \ c_2 \ c_3 \ c_4 \ c_5 \ c_6\|_*, \tag{10}$$

is the column of polynomial coefficients (8).

A set of discrete values of the function $F_m[\gamma, r_m]$, which will be referred to as a TF template, is formed on the basis of the values of the corresponding TF. The number of such values should be six, which corresponds to the number of unknown coefficients in (8). The interpolation procedure begins with the search for such tabular values of the arguments γ_{tb} and r_{m6} , which have the smallest deviations from the given (known) values of the arguments $\min|\gamma_{tb} - \gamma|$ and $\min|r_{m6} - r_m|$. Such a pair of argument values will be called the central node of TF. Subsequently, the TF template is supplemented with neighboring nodes according to the rule that is schematically depicted in Figure 7. In the figure, the TF $F_m[\gamma, r_m]$ is shown in the form of a table, and the values of its arguments included in the template, depending on the location of the central node, are shown in the form of hatched cells.

The Taylor matrix is formed according to the following rule: any row of this matrix with an arbitrary number k is a Taylor’s series (9) written for the nodal values of the TF arguments with the number k ,

$$T = \begin{pmatrix} 1 & \gamma_1 & r_{m1} & \frac{\gamma_1^2}{2!} & \gamma_1 r_{m1} & \frac{r_{m1}^2}{2!} \\ \vdots & & & & & \\ 1 & \gamma_6 & r_{m6} & \frac{\gamma_6^2}{2!} & \gamma_6 r_{m6} & \frac{r_{m6}^2}{2!} \end{pmatrix}. \tag{11}$$

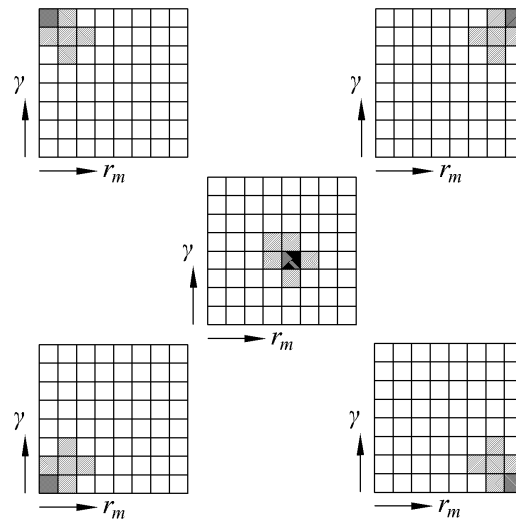


Figure 7. Formation of the TF template.

The values of TF corresponding to the nodal values of the arguments are combined into a column vector

$$\vec{F}_{mt} = \|F_{m1} \dots F_{m6}\|_* \tag{12}$$

After solving the vector equation

$$T \cdot \vec{c} = \vec{F}_{mt}, \tag{13}$$

relative to the vector unknown \vec{c} , a column of polynomial coefficients is obtained (8).

Therefore, the algorithm for obtaining the interpolated value of the TF $F_m[\gamma, r_m]$ for arbitrary given values γ_z and r_{mz} consists of sequentially performing the following operations:

- calculation of the elements of the Taylor’s matrix (11);
- formation of a column of TF values (12);
- solutions of the linear vector Equation (13) regarding the unknown \vec{c} ;
- calculating the value of the Taylor’s series (9) based on $\gamma = \gamma_z, r_m = r_{mz}$;
- calculating the interpolated value of TF as a multiplication $\vec{T}[\gamma_z, r_{mz}] \cdot \vec{c}$.

It should be noted that the interpolated values of the other components of the vector TF \vec{S}_m , namely, the force direction α_m and the torque M_m , are similarly found from the corresponding scalar TF $\alpha_m[\gamma, r_m] M_m[\gamma, r_m]$.

This algorithm is suitable for TFs containing an arbitrary number of nodes with an arbitrary mutual location of nodes in the template.

Verifying its operability and evaluating the accuracy of the interpolation of the above-mentioned vector function $\vec{S}_m(\vec{z})$ was conducted based on the TFs obtained by the methods described in Section 6.

The dependence of the interpolated value of the force modulus \bar{F}_m on the angular displacement γ is shown in Figure 8a with a solid-line curve. In this case, the angle of inclination of the longitudinal axis of the millstone was $\alpha_m = 90^\circ$. The dashed curves shown on the same graph are similar dependencies that correspond to the deviation of the angular displacement within the limits $\pm 5^\circ$. Here, it should be noted that the magnitudes of forces and moments are related to the unit length of the millstone in the direction normal to the calculation plane. This is due to the two-dimensional formulation of the problem of calculating the magnetic field. Therefore, their dimensions are N/m and Nm/m, respectively.

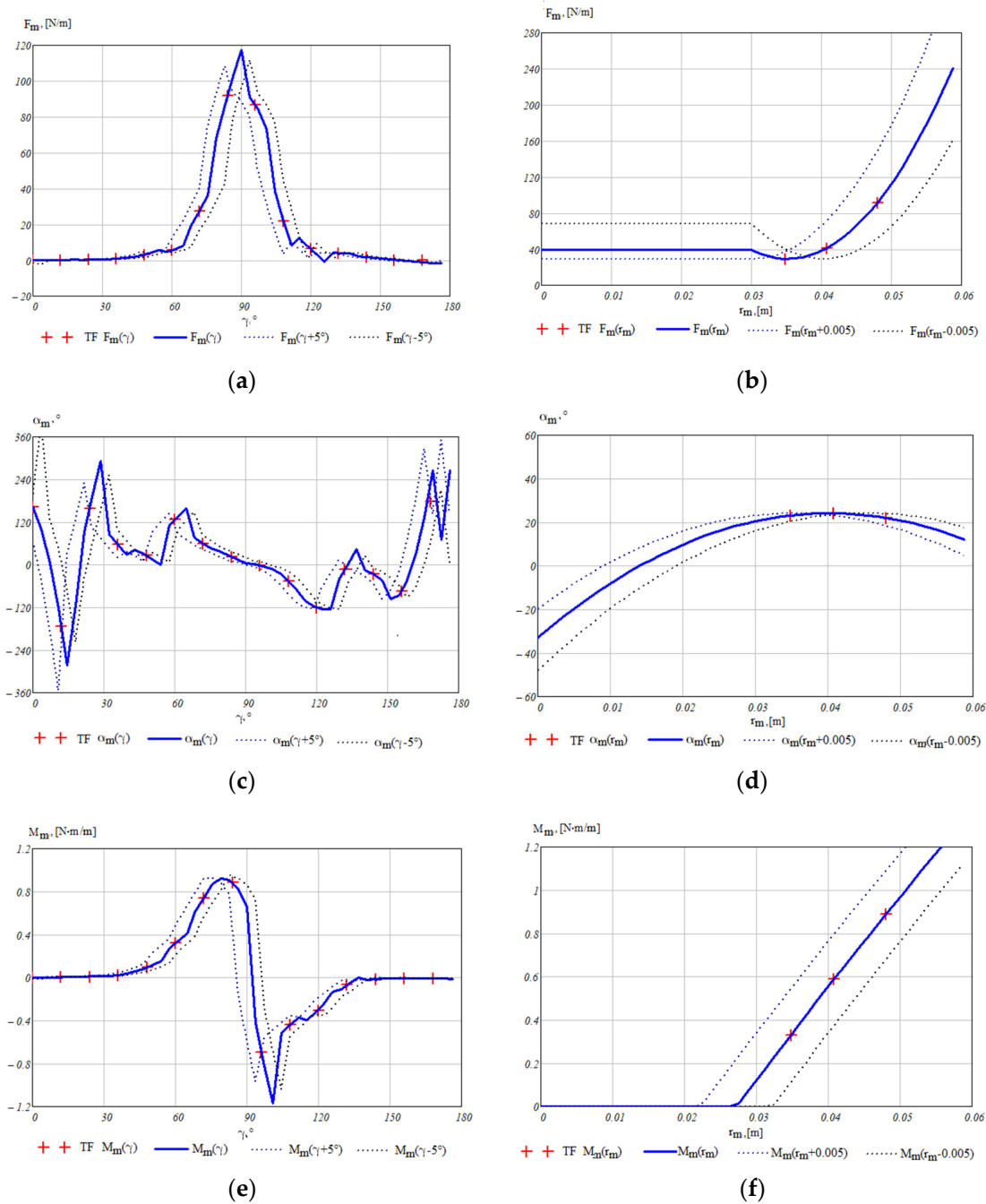


Figure 8. Interpolation dependencies for TF: (a) $F_m[\gamma]$ for $r_m = 0.048$ mm; (b) $F_m[r_m]$ for $\gamma = 84^\circ$; (c) $\alpha_m[\gamma]$ for $r_m = 0.048$ mm; (d) $\alpha_m[r_m]$ for $\gamma = 84^\circ$; (e) $M_m[\gamma]$ for $r_m = 0.048$ mm; (f) $M_m[r_m]$ for $\gamma = 84^\circ$.

The graph in Figure 8b contains the dependence of the modulus of the same force \bar{F}_m on length of the radius vector r_m (solid-line curve) and similar dependencies in case of deviations r_m within ± 5 mm (dashed curves).

The graphs of Figure 8c,d are interpolation dependencies of force direction α_m on the angular displacement γ and the length of the radius vector r_m , respectively. Figure 8e,f is the dependencies of the torque M_m on the above-mentioned arguments. The dashed curves in these graphs are obtained for the same deviations of the arguments as in the case of the dependencies for the force modulus F_m .

In all graphs in Figure 8, '+' symbols mark the nodal values of the TF.

8. Mathematical Model of the Dynamics of Millstone Movement in the MM Working Chamber

All the preliminary mathematical processing conducted is aimed solely at preparing input data for a mathematical model that calculates indicators of the movement of millstones and WS particles located in the rotating magnetic field of the inductor. Any movements of these elements were considered by us to be planar movements, that is, they were described by functions of only two spatial coordinates.

The differential equations of motion of the center of mass of a two-dimensional body and the equation of moments for relative motion around an axis passing through the center of mass perpendicular to the plane of motion are as follows

$$\frac{d^2 x_m}{dt^2} = \frac{\sum_{i=1}^n F_{ix}}{m}; \quad \frac{d^2 y_m}{dt^2} = \frac{\sum_{i=1}^n F_{iy}}{m}; \quad \frac{d\omega_m}{dt} = \frac{1}{J} \sum_{i=1}^n M_z(F_i) = \frac{M_z}{J}; \quad \omega_m = \frac{d\phi}{dt}, \quad (14)$$

where x_m , y_m and ϕ —coordinates of the center of mass and the angular position of the millstone; m is the mass of the millstone; J , $M_z(F_i)$, M_z is the moment of inertia, the moment of force F_i and the main moment of all external forces relative to the axis passing through the center of mass; ω_m is the angular speed.

The mathematical formulation of this problem takes into account the forcing forces, the magnitude and direction of which were calculated based on the interpolation procedure of the vector TF $\vec{S}_m(\vec{z})$, namely, the modulus of the force, its direction and torque. On the basis of the obtained values, which were updated at each time integration step, force projections \bar{F} and \bar{F}_o were determined (Figure 2). The values of the projections \bar{F}_o were calculated according to the formulas

$$F_{ox} = \pm \frac{2M_m}{l_m} \sin(\alpha_m + \gamma_m); \quad F_{oy} = \pm \frac{2M_m}{l_m} \cos(\alpha_m + \gamma_m). \quad (15)$$

The points of their application are marked in this figure with numbers 1 and 3.

System (14) consists of four equations and contains four unknown functions: $x_m(t)$, $y_m(t)$, $\phi(t)$, and $\omega_m(t)$. It constitutes the content of the mathematical formulation of the problem of calculating the trajectories of the planar motion of a rigid body of arbitrary shape which is affected by action of external forces and moments. An algorithm for solving such a problem for a system of interacting bodies using the finite element method is considered in [31]. Its software implementation is performed in the Ansys LS-DYNA software complex [32] in the APDL (Ansys Parametric Design Language) programming language.

To process contact interactions within the system of bodies, such as touching, sliding, etc., the method of kinematic restriction is used, the essence of which is to block the degree of freedom of nodes responsible for normal movements in relation to the contact line. To preserve the efficiency of algorithm of the method of explicit numerical integration over time of systems of type (14), the masses of the bodies are concentrated (scaled) to such a limit that only the main degrees of freedom of each node [33] remain connected.

In order to verify the performance of the created model and to assess its level of adequacy, the trajectories and other indicators of the movement of a set of five millstones and eight WS particles, located in a WC with a diameter of 120 mm, were calculated. Ferromagnetic millstones are subjected to the force of the rotating magnetic field created by the inductor, which was mentioned and described in the mathematical experiment for calculating the field of magnetic forces in Section 6. The dimensions of the millstones are $d_m = 1.5$ mm and $l_m = 13.5$ mm. The diameter of the particles for grinding is ≈ 9 mm.

This and all subsequent mathematical experiments were conducted under the condition that WS particles are in a liquid with an estimated density of 15% of water density. This method made it possible, on the one hand, to take into account the influence of hydrodynamic resistance forces (6), and on the other hand, to accelerate the output of

the multicomponent system to a quasi-steady mode of operation and reduce the total calculation time.

At the initial moment of time, the millstone and WS particles were located evenly around the circle with diameters of 43.8 mm and 54 mm, respectively. The angle of rotation of the millstone axes α_m at the beginning of the calculation was 30° . The frequency of rotation of the inductor is 2000 rpm. The estimated mass of the millstone and the WS particles are 0.18 g and 0.11 g, respectively. Their relative location for $t = 0.00$ s is shown in Figure 9a.

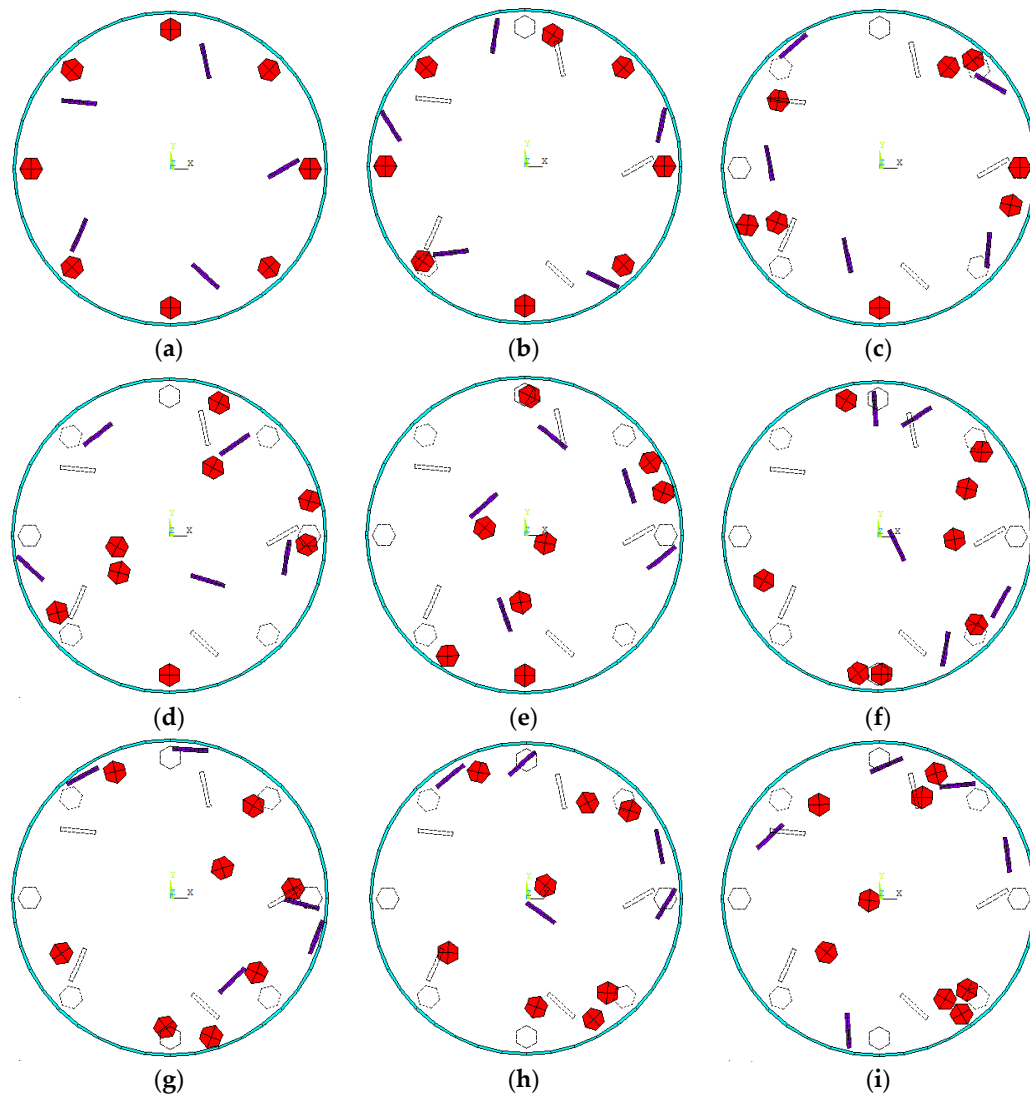


Figure 9. Position of millstones and WS particles in RK for different moments of time: (a) 0.00 s; (b) 0.02 s; (c) 0.04 s; (d) 0.06 s; (e) 0.08 s; (f) 0.10 s; (g) 0.12 s; (h) 0.14 s; (i) 0.16 s.

The vectors of the initial velocities for all millstones, at the moment of time $t = 0$, were the same and contained only the tangential component of the velocity $v_{\tau i} = 9.2$ m/s ($i = 1, \dots, 5$). The WS particles were in a state of rest.

Figure 9b–i illustrates the sequential change in the positions of the millstones and WS particles during the interaction process. In these figures, the initial position of all elements of this system is indicated by dashed contours for better visualization.

In order to quantitatively assess the movement indicators in Figure 10, hodographs of the radius vectors of the centers of mass and hodographs of point 1 (see Figure 2) of

millstones with the numbers $i = 1$ and 3 are constructed. This makes it possible to track not only the position of a single millstone, but also its rotation around its center of mass.

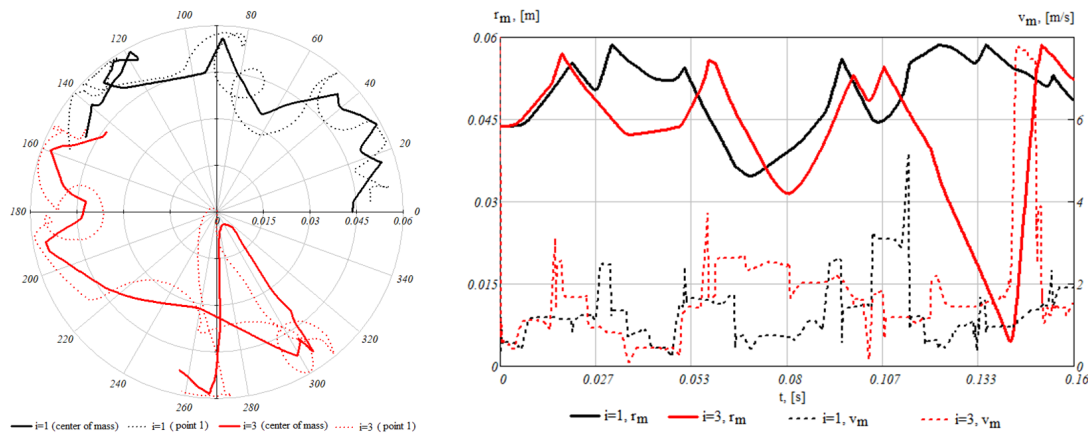


Figure 10. Indicators of movement of millstones 1 and 3.

Figure 10b shows the dependence of the displacement r_m modules and the velocity v_m of millstones with conditional numbers $i = 1$ and 3 in one coordinate plane. This makes it possible to track the moments of their impacts and collisions.

Millstone 1 begins to slowly move upwards under the influence of the velocity vector of the initial condition. The influence of the magnetic field of the inductor at this moment is insignificant, since the angular displacement $\gamma \approx 90^\circ$. Then, this millstone falls into the area of action of the magnetic field of the approaching pole of the inductor, leading to its attachment to the wall of the WC and elastic rebound from it. This happens three times in the zone $\gamma_m \approx 20^\circ \div 40^\circ$ and at moments of time $t \approx 0.025 \div 0.050$ s. At the same time, this millstone moves along a circular path in the direction of rotation of the mill inductor, i.e., counter-clockwise. Then, it collides with WS particles, in particular due to rotation around its own center of mass under the action of the magnetic moment M_m . This rotation is clockwise.

Continuing to rotate around its own center, millstone 1 hits the wall of the WC four times in the area $\gamma_m \approx 90^\circ$ and $t \approx 0.09$ s. Then, it collides with another millstone ($i = 5$) and loses the accumulated kinetic energy. It continues almost rectilinear movement under the influence of the magnetic field and again bumps into the wall in the zone $\gamma_m \approx 130^\circ$. After that, it slides along it in the opposite direction to the direction of inductor rotation. It stops in a moment ($t \approx 0.13$ s) and changes the direction of movement. The rotation of this millstone around its own center is also restored.

Millstone 3 almost immediately falls under the influence of one of the poles of the inductor, which is explained by the smaller value of the angular displacement $\gamma \approx -45^\circ$. As a result, it is immediately attached to the WC wall, hits and bounces off it ($\gamma_m \approx 170^\circ$, $t \approx 0.018$ s). Afterwards, it begins to rotate clockwise around its center of mass. All this is accompanied by numerous collisions with WS particles and the WC wall. After another such collision, the millstone slowly moves in a radial direction $\approx 300^\circ$ to the center of the WC, where the influences of the magnetic force F_m and moment M_m are insignificant. After a short pause, at the moment of time $t \approx 0.14$ s, the millstone moves in the radial direction $\approx 270^\circ$ with noticeable acceleration, almost without turning, until another collision with the WC wall.

In the graphs in Figure 10, it can be seen that the moments of breaks in the displacement functions correspond to such moments with breaks in the speed functions; the duration of the rise or fall of fronts of the trajectories corresponds to time intervals during which the speed of the millstone practically does not change. Oscillations of the speed functions with a relatively small amplitude can serve as an indirect confirmation of the fact of impact interaction between the millstones and the WC walls due to friction between them and, as a

result, continuation of the grinding process even in quasi-steady modes, when the angular velocities of all elements of the system are approximately the same.

The results of this study do not contradict physical ideas about the course of interaction of ferromagnetic millstones moving in the rotating magnetic field of the PM inductor with WS particles and WC walls. Therefore, it can be stated that the created mathematical model for calculating the trajectories of the millstones in the WC of the magnetic mill is adequate within the accepted assumptions. The calculation results obtained with this model can be used to further evaluate the performance of the grinding/mixing process.

To demonstrate the operation of the above-mentioned model with a larger number of millstones and WS particles, Figure 11 shows the WC in which there are 390 millstones and 70 WS particles. The diameter of a millstone in this experiment was 1 mm, and its length was 7 mm.

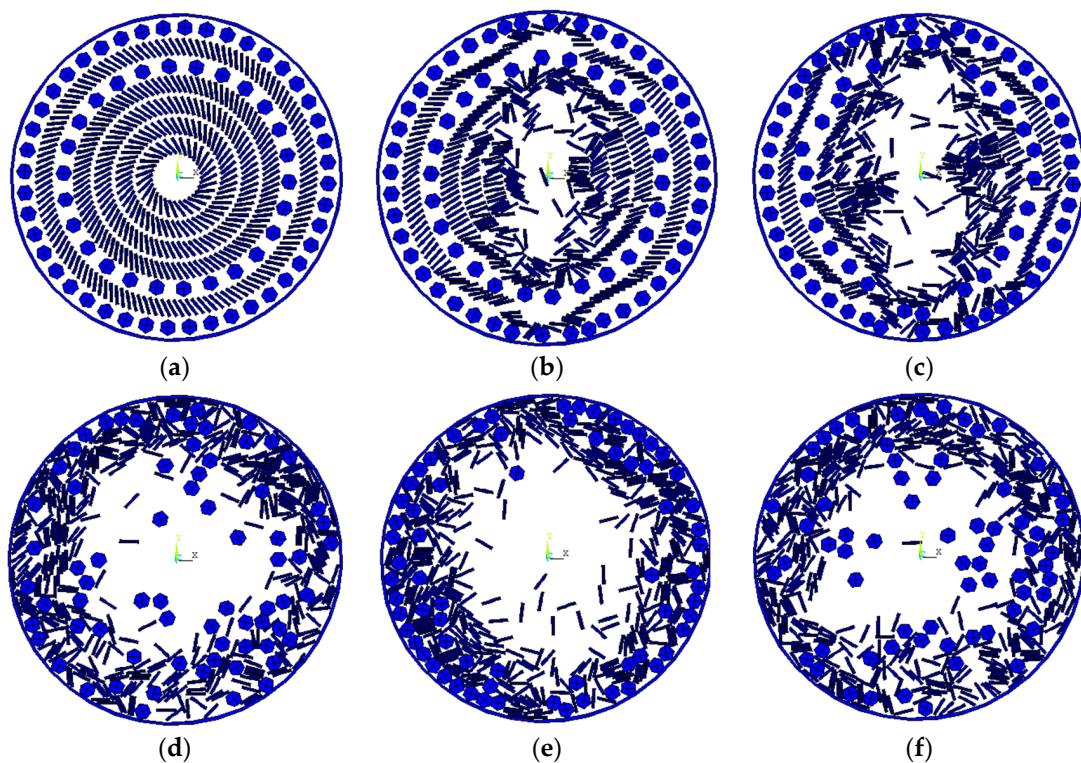


Figure 11. Demonstration of operation of the mathematical model (a) 0.00 s; (b) 0.002 s; (c) 0.004 s; (d) 0.014 s; (e) 0.02 s; (f) 0.16 s.

The calculation was performed on a personal computer with an Intel® Core™ i5-8250U 3.60 GHz processor; 32 GB of RAM, and its duration was ≈ 1.5 h.

9. Estimated Performance Indicators of the Magnetic Mill

Having analyzed the results of our mathematical and physical experiments and having taken into account studies [2–4], we have come to the conclusion that the most important factors directly affecting the amount of grinding material obtained per unit of time are the number of impacts of the millstones and the impulse of force of these impacts. Therefore, it can be assumed that these indicators, together with the force interaction indicators (Section 6), connect the design parameters of the mill with its productivity.

The total number of blows of millstone impacts k_u for a fixed period of time was calculated taking into account the number of millstone impacts between themselves, with WS particles and the WC walls. This indicator was defined as

$$k_u = \sum_{i=1}^{n_m} k_{ui}, \quad (16)$$

where k_{ui} —is the number of impacts of i -th millstone for a fixed period of time Δt ($i = 1, \dots, n_m$); n_m —is the number of millstones in the working chamber.

The value k_u , primarily, depends on the level of filling of the WC with millstones, since it is obvious that the number of impacts increases only as a result of the increase in the number of millstones. On the other hand, this value depends on the rotation frequency and the intensity of the magnetic field, the ratio of the sizes of the millstones and the WC, as well as on a number of physical and mechanical properties of the materials involved in the grinding process.

The calculation of the number of impacts was performed on the basis of a numerical analysis of millstone trajectories and their velocities, obtained as solutions of the system of algebraic differential equations of the model described in Section 8. The calculation is based on determination of one of the kinematic characteristics of a material point, which is called a jerk. This is a vector quantity that describes the rate of change of the acceleration of a point; consequently, it is the third time derivative of its radius vector. In our case, the jerk was calculated as the second derivative of the velocity vector of the i -th millstone [13]

$$\vec{G}_i = \frac{d^3 \vec{r}_{mi}}{dt^3} = \frac{d^2 \vec{v}_{mi}}{dt^2}. \tag{17}$$

The jerk modulus of the i -th millstone at the moment of time $t = t_k$ (at the k -th step of integration) is determined by its projections:

$$G_i|_{t=t_k} = \sqrt{G_{xi}^2 + G_{yi}^2}. \tag{18}$$

Projections G_{xi} and G_{yi} were determined using a mathematical apparatus similar to that used for the interpolation of the TF (Section 7). Tabular functions of projections of the speed of movement of the center of the i -th millstone mass $v_{xi}(t)$ and $v_{yi}(t)$ at some time interval were represented in the form of Taylor’s polynomials of the 2nd degree. Then, the expression of the x -projection of speed, in scalar and vector form, is

$$v_{xi}(t) = c_1 + c_2 t + c_3 \frac{t^2}{2!}, \quad \vec{v}_{xi}(t) = \vec{T}[t] \vec{c}, \tag{19}$$

where $\vec{T}[t] = \left\| 1 \quad t \quad \frac{t^2}{2!} \right\|$ is a Taylor’s series of the 2nd degree with one independent variable; and $\vec{c} = \left\| c_1 \quad c_2 \quad c_3 \right\|_*$ is a column of polynomial coefficients.

Such values of the tabular function $v_{ix}(t)$ were chosen as to correspond to the moment of time t_k when the second derivative is calculated (17). They are combined into a column

$$\vec{v}_{xi} \Big|_{t=t_k} = \left\| v_{x,k} \quad v_{x,k-1} \quad v_{x,k-2} \right\|_*, \tag{20}$$

where $v_{x,k}, v_{x,k-1}, v_{x,k-2}$ are the values of the x -projections of the velocity at the moments of time t_{k-1}, t_{k-2} , respectively.

The x -projection of the jerk in this case is equal to

$$G_{xi} \Big|_{t=t_k} = \frac{d^2 v_{xi}}{dt^2} = \vec{T}[t] D^2 T^{-1} \vec{v}_{xi}, \tag{21}$$

where

$$T = \left\| \begin{matrix} 1 & t_k & \frac{t_k^2}{2!} \\ 1 & t_{k-1} & \frac{t_{k-1}^2}{2!} \\ 1 & t_{k-2} & \frac{t_{k-2}^2}{2!} \end{matrix} \right\|, \quad D = \left\| \begin{matrix} 0 & 1 & 0 \\ 0 & 0 & 1 \\ 0 & 0 & 0 \end{matrix} \right\| \tag{22}$$

are the Taylor’s matrix and the Taylor’s series differentiation matrix, respectively.

The projection of the jerk G_{yi} was found in a similar way. After that, the jerk modulus was determined according to (18) and its effective value at the required time interval Δt

$$G_i^{rms} = \sqrt{\frac{1}{\Delta t} \int_t^{t+\Delta t} G_i^2 dt} = \sqrt{\frac{1}{\Delta t} \sum_{k=1}^{KI} (G_{xik}^2 + G_{yik}^2) \cdot (t_k - t_{k-1})}, \tag{23}$$

where KI —is the number of time integration steps in the selected time interval Δt .

Based on the comparison of the effective value G_i^{rms} with the current value G_i the number of impacts of the i -th millstone KU_i was calculated taking into account the condition

$$G_i \geq G_i^{rms} \Rightarrow KU_i = KU_i + 1. \tag{24}$$

The next indicator of the productivity of the grinding/mixing process is the average value of the pulse of the millstone impact force

$$S_{us} = \frac{1}{n_m} \sum_{i=1}^{n_m} S_{usi}, \tag{25}$$

where S_{usi} is the average force impulse of the i -th millstone for a fixed period of time Δt .

The average value of the force impulse of the i -th millstone

$$S_{usi} = \frac{1}{\Delta t} \int_t^{t+\Delta t} S_i dt = \frac{1}{KU_i} \sum_{j=1}^{KU_i} S_{ij}, \tag{26}$$

where S_i is the force impulse of the i -th millstone;

S_{ij} is the force impulse of the i -th millstone at the moment of the j -th impact ($j = 1, \dots, KU_i$). This value is determined by the expression

$$S_{ij} = m_i \sqrt{(v_{xi}^{end} - v_{xi}^{start})^2 + (v_{yi}^{end} - v_{yi}^{start})^2}, \tag{27}$$

where m_i is the mass of the i -th millstone; $v_{xi}^{start}, v_{yi}^{start}$ are projections of the speed of movement of the mass center of the i -th millstone at the time of starting the j -th jerk; $v_{xi}^{end}, v_{yi}^{end}$ are projections of the speed of movement of the mass center of the i -th millstone at the time of finishing the j -th jerk.

Based on the calculated values k_u and S_{us} , we tried to outline the integral performance indicator [14]. However, the method of its determination needs more careful study and experimental confirmation.

Let us illustrate the application of the proposed method of calculating MM performance indicators using the example discussed in Section 8 (Figure 10).

The duration of the transient process in this mathematical experiment was 0.16 s. The average and current values of the calculated indicators (displacements, speeds, jerk) were determined during the time interval $0.14 \div 0.16$ s. It corresponded to one complete turn of the inductor rotating at a frequency of 2000 rpm.

Figure 12a shows the time dependence of the modules and displacement projections r_{m3}, x_{m3}, y_{m3} , and the speed v_{m3}, v_{x3}, v_{y3} of the center of mass of the 3rd mill ($i = 3$).

Hereinafter, expression (21) was alternately applied to tabular functions $v_{x3}(t)$ and $v_{y3}(t)$ in order to obtain projections of the jerk G_{xi}, G_{yi} and its modulus G_i (18). Figure 12b shows the time dependence of the jerk modulus of the 3rd millstone and the level corresponding to the root mean square value of this value.

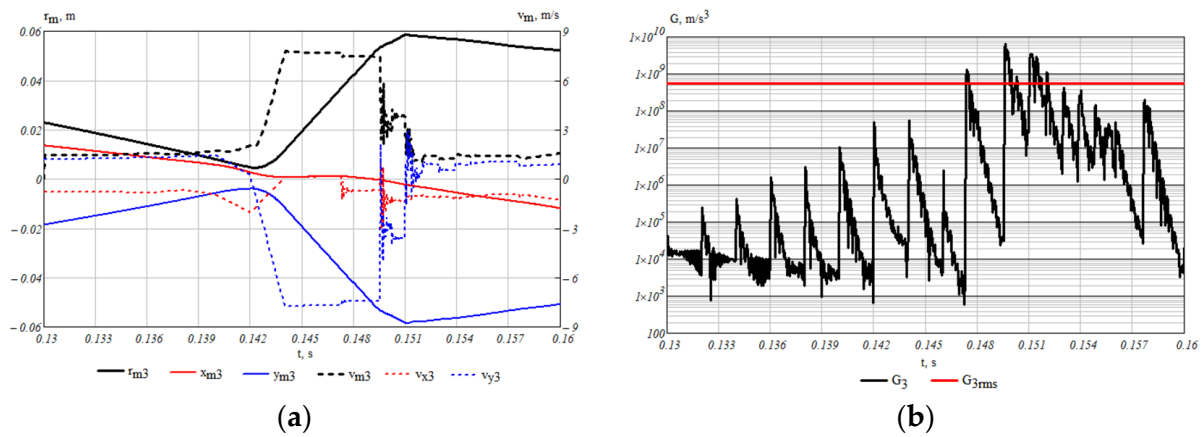


Figure 12. Dependencies on time for the millstone ($i = 3$): (a) displacement and velocity projections and modules; (b) jerk modulus.

The scaling-up of the time axis in Figure 13 made it possible to monitor the correspondence between the jump-like change in speed projections and the appearance of jerk oscillations $G_3(t)$. This figure also shows the initial and final velocities $v_{x3}^{start}, v_{y3}^{start}, v_{x3}^{end}, v_{y3}^{end}$ at the time of one of the jerks ($t = 0.1496$ s). These values were used to calculate the force impulse of the millstone ($i = 3$) according to (27) at the moment of this impact. Its value was 1.1587×10^{-3} Ns. The average force impulse of the 3rd millstone in the aforementioned time range was 2.723×10^{-4} Ns. Processing of modeling results based on principle (24) revealed 6 impacts in the time interval $0.148 \div 0.152$ s.

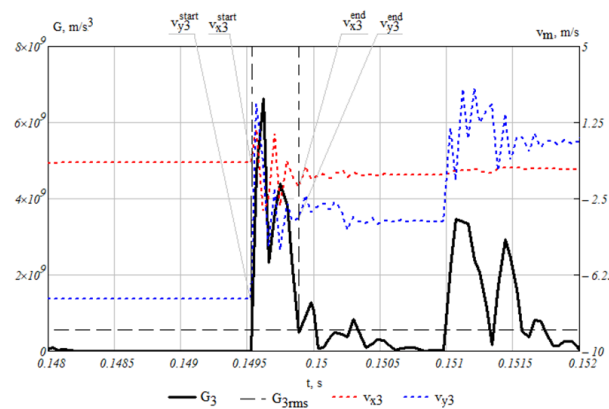


Figure 13. Time dependence of velocity projections and the jerk module for the millstone ($i = 3$).

For the entire set of 5 millstones (Figure 9), the total number of impacts was 20, and the average force impulse of these collisions was 8.551×10^{-5} Ns.

10. Verification of the Model Using a Physical Experiment

The adequacy of the approach proposed in Section 8 for calculating the movement features of ferromagnetic millstones under the action of ponderomotive forces in a rotating magnetic field was verified by comparing the obtained results with the results of experimental studies on the physical model of the MM. The characteristics of millstone movement were considered to be their trajectories in the WC plane, the time dependence of spatial coordinate projections of the position of the mass center of individual millstones and other characteristic points of this system.

A photo of the laboratory installation intended for conducting the above-mentioned study is shown in Figure 14. It consists of an inductor with PM 1, a ceramic WC 2 with a volume of 1130 cm³, a driving engine 3 together with switching equipment and a control

system 4, a supporting and rotating device 5, a tripod for installing the recording equipment 6, a lighting system 7, and supporting and body parts 8.



Figure 14. Laboratory setup for studying the MM: 1—inductor with PM; 2—working chamber; 3—driving engine; 4—supervision system; 5—support arrangements of the supporting and rotating device; 6—tripod; 7—illumination lamp; 8—bed plate.

The entire installation is powered by a single-phase network with a voltage of 230 V and commercial frequency.

The pole tips of the MM model inductor are made of sheets of M600-50A electrical steel with a thickness of 0.5 mm, insulated on both sides with an oxide film. Sheets of the tips are assembled into cores and bonded with an epoxy compound. The poles of the inductor are made of composite material based on NdFeB (residual induction 1.2 T, coercive force 800 kA/m). The pole tips and poles are mounted in the sockets of the body frame, which is rotated by the driving engine. The structural elements of this body frame are made of ABS plastic by 3D printing.

The WC is installed in the inductor bore with a diameter of 140 mm. It is made of silicon ceramics. Its wall thickness is 5 mm. The angular and radius scales are applied to the bottom of the WC, which makes it possible to approximately determine the current position of the millstones. The inductor together with the poles and the driving mechanism, the WC and the research video recording system are mounted on the supporting element of the structure—a bed plate made of artificial stone. All of this is installed in a frame made of aluminum profiles.

The supervision system of the laboratory installation provides for smooth adjustment of the rotation frequency of the driving engine in the range of $0 \div 5000$ rpm, illumination of the experimental area at the level of 2000 lx, and automatic start and stop of video recording of the grinding process.

The experimental study consisted in comparing the characteristics of the millstone movement obtained by direct identification using video recording (Figure 14) with similar calculated characteristics determined using a mathematical model (Section 8). The obtained results of the physical experiment were also used for a critical assessment of the assumptions underlying the aforementioned model, that is, the movement of millstones is considered to be plane movement, and the longitudinal axis of a millstone is considered to be oriented along the lines of force of the magnetic field.

At the beginning of the experiment, five identical cylindrical steel millstones were placed in random positions in the WC. Then, the driving engine was launched, which was rotating the 2-pole inductor (Figure 3) with a frequency of 2500 rpm around the WC body frame. The dimensions of the millstones used in the experiment are as follows: diameter: 1.3 mm; length: 12.0 mm. After accelerating to a fixed rotation frequency, in 10–20 s, the video camera was turned on in the recording mode of 1000 frames per second and the process of movement of the millstones in the magnetic field of the inductor was recorded.

The duration of the video recording in real time was ≈ 2.5 s. The obtained video recording was used to determine characteristics of the movement of millstones in real conditions of conducting a physical experiment.

Specialized software Tracker 5.1 (OSP) [34] was used to process the results of this experiment, in particular to monitor the behavior of millstones in real time, their reference to the coordinate system, size calibration, determination of positions, values of velocity projections, etc.

Time alignment of the calculation process with the experimental process took place with the help of the initial condition obtained on the basis of analysis of the video recording of the experiment, using the aforementioned Tracker software. This condition contains information about the initial inclination of the axis $+d$ of the magnetic system of the inductor ($\gamma_i = -115.0^\circ$, Figure 2), the initial positions of the five millstones for $t = 0$ s, and their linear velocities at that moment. All this information is presented in Table 1.

Table 1. Initial condition.

Number of the Millstone	Radius Vector r_m, m	Angular Coordinate of the Millstone $\gamma_m, ^\circ$	Angle of Rotation $\alpha_m, ^\circ$	Module of the Velocity Vector $v_m, \text{m/s}$	Direction of the Velocity Vector $\alpha_v, ^\circ$
1	0.0361	-141.2	-35	0.7066	104.4
2	0.0325	126.9	-25	1.9329	-59.9
3	0.0513	82.7	45	0.4190	-68.4
4	0.0252	79.1	100	2.0095	-105.7
5	0.0242	12.5	100	1.3913	-101.4

A comparison of five frames of the video recording and images obtained on the basis of the calculation, corresponding to the moments of time 0.0 s, 0.03 s, 0.06 s, 0.09 s, and 0.12 s, is shown in Figure 15. The numbering of millstones (from 1 to 5) is conventionally shown there.

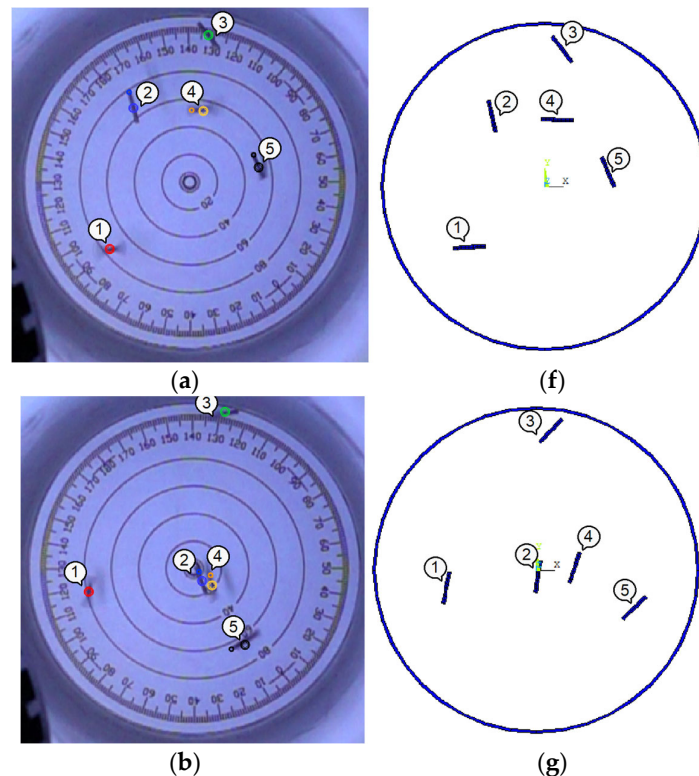


Figure 15. Cont.

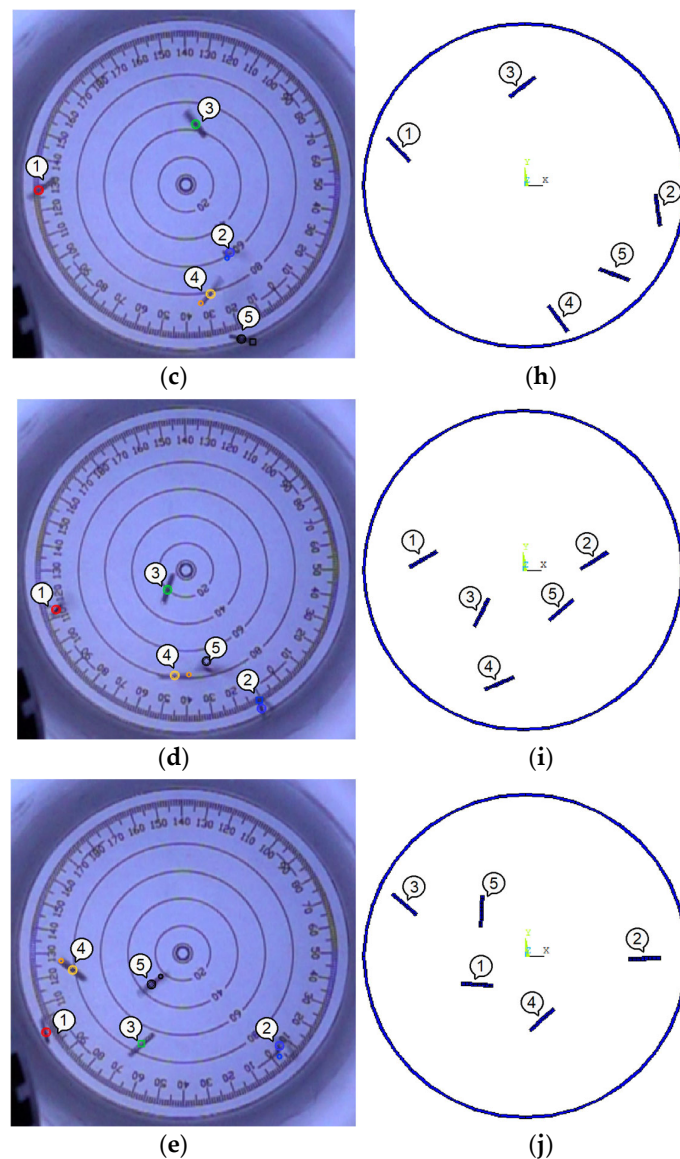


Figure 15. Positioning of millstones in the WC at moments of time: (a,f) 0.0 s; (b,g) 0.03 s; (c,h) 0.06 s; (d,i) 0.09 s; (e,j) 0.12 s; determined on the basis of the experiment (a–e); based on the calculation (f–j).

Direct analysis of the video recording of the process showed that the direction of rotation of a millstone around its own axis is opposite to the direction of rotation of the inductor field. This is due to several reasons. Firstly, it is due to the relatively large difference between the rotation frequency of the field and the rotation frequency of the mill around the WC axis. The second reason is the displacement of the rotation axis of each millstone relative to the inductor axis, as a result of which the force effect on the opposite ends of the millstone is different both in magnitude and direction.

The trajectories of millstones with numbers 1, 3 and 5 obtained by experimental and calculation methods are compared in Figure 16. The graphs in the polar coordinate system show hodographs of the vector \vec{r}_m and the radius vector of the point of application of one of the pair of forces \vec{F}_o , namely point 1 (Figure 2). This dependence reflects the rotational movement of the millstone around its own center of mass.

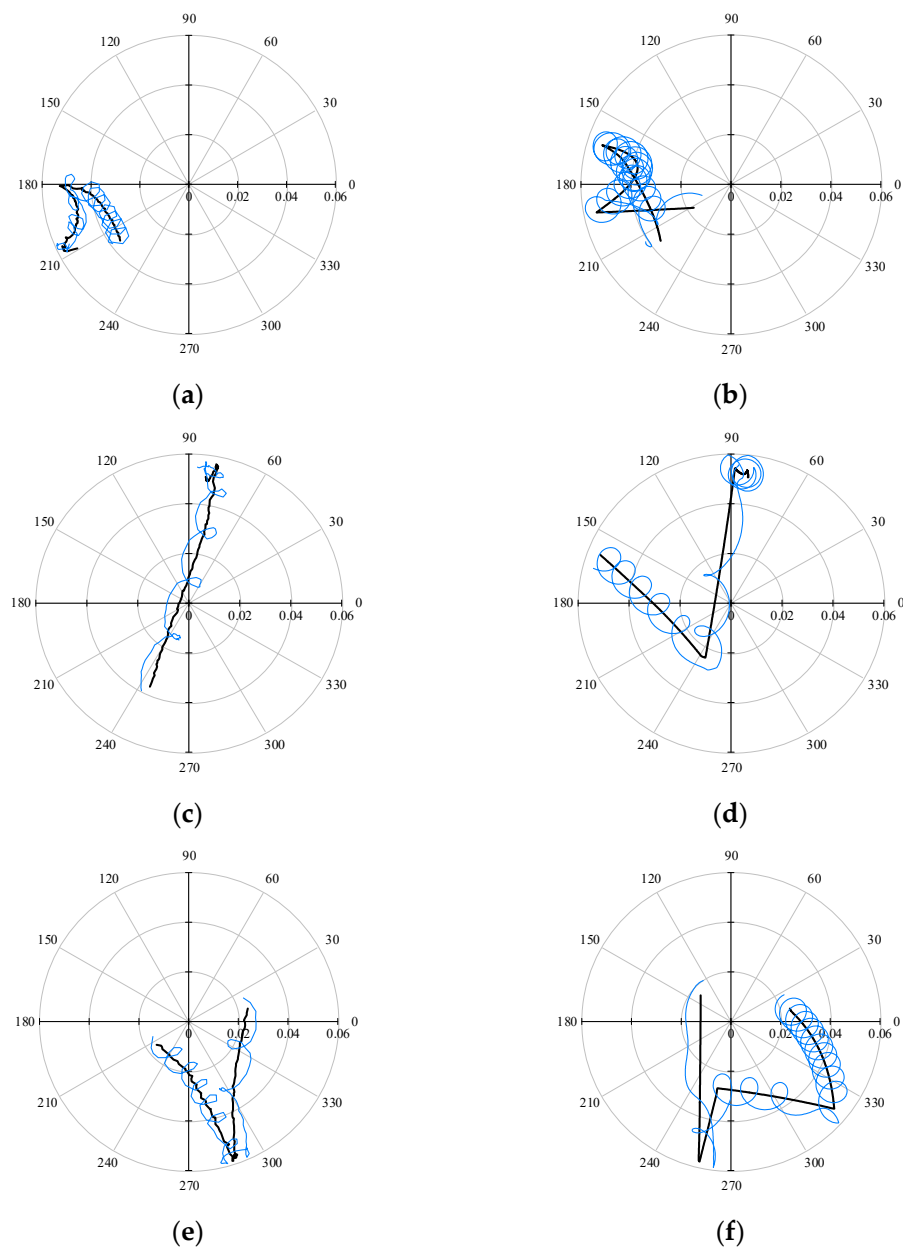


Figure 16. Trajectories of characteristic points of millstones 1 (a,b), 3 (c,d), 5 (e,f) obtained on the basis of: experiment (a,c,e); calculation (b,d,f).

As can be seen from this comparison, the calculated trajectories mainly reflect the characteristic features of the behavior of ferromagnetic millstones in a rotating magnetic field. A movement around the center of the WC in the direction of rotation of the magnetic field and rotation around an axis passing through the center of mass is observed. On the other hand, there are also significant differences between the calculation and the experiment, in particular, in the shapes of the trajectories and in the instantaneous values of linear velocities and accelerations. This is due to a number of reasons:

- at certain moments of time, the movement of the millstones ceases to be flat, inevitably leading to a change in the time intervals between the events of contact interactions—touches, impacts, and collisions;
- rotation frequencies of millstones around their own centers of mass, on average, are not the same and differ by 50–100%;

- the frequency of rotation of the magnetic field adopted for the calculation turned out to be higher (by 20–30%) than the frequency of rotation of the inductor in the physical experiment;
- mutual magnetization of particular millstones is observed; this is accompanied by formation of structures whose shapes and dimensions differ from those laid down in the model, which radically changes the shape of the trajectory of such a newly created ‘double’ dipole and its dynamic characteristics;
- the redistribution of the energy of elastic impacts between the millstones and the wall of the ceramic WC in physical and mathematical experiments does not occur in the same way, which can be explained by the discrepancy between the physical and mechanical properties of the materials from which the real WC is made and the properties that are included in the model.

It should be emphasized that one of the tasks of our research was to create an adequate computational tool that would allow for a quantitative assessment of the impact of design parameters of the MM on the performance of the grinding process. The calculation of the dynamics indicators of millstone movement is only one of the intermediate stages in achieving this goal, and the exact coincidence of the trajectories of millstone movement with the experiment is not a mandatory condition in this case. Therefore, at this stage of the research, in our standpoint, a compromise between the adequacy of the model and its complexity, the demand for computing resources and the laboriousness of development and software implementation have been achieved.

Summarizing the above, it can be stated that the comparative analysis of experimental and calculated data shows that the created mathematical model mainly takes into account all the necessary factors affecting the movement of millstones in a rotating magnetic field, and the experimental and calculated characteristics of the movement, such as the trajectories of the centers of mass, their velocities and accelerations, correlating with each other.

11. Conclusions

A mathematical model for calculating the trajectories of movement of ferromagnetic millstones in a rotating magnetic field confined by the space of the working chamber was developed. Its algorithm is suitable for the study of working chambers and millstones of any size and shape. The model is designed based on equations of the dynamics of the movement of bodies in a two-dimensional setting (the so-called plane movement), which made it possible to take into account the influence of:

- contact interaction of the millstone with the particles of the substance being ground/mixed;
- hydraulic resistance forces acting on moving elements during this interaction;
- dry friction.

The preparation of the input information for the above model, which is conducted based on the calculation of the ponderomotive force field in a two-dimensional formulation, adequately reflects the influence of the actual configuration of the inductor magnetic wire, its saturation and saturation of ferromagnetic millstones, in the interrelationship of these factors.

The developed method of identification of moments of millstone collision with other elements of the system is based on the calculation of the jerk vector. It makes it possible to calculate the average number of impacts of millstones and the average impulse of the force of these impacts. These indicators quantitatively characterize the productivity of the grinding/mixing process of a real technical system containing a magnetic mill.

Author Contributions: Conceptualization, D.C.; methodology, D.C. and O.M.; software, O.M.; validation, D.C., S.B. and P.D.; formal analysis, D.C. and O.M.; investigation, D.C., O.M., S.B. and P.D.; resources, D.C.; data curation, O.M. and D.C.; writing—original draft preparation, D.C.; writing—review and editing, D.C., O.M., P.D. and S.B.; visualization, O.M.; supervision, D.C.; project adminis-

tration, D.C.; funding acquisition, D.C. and O.M. All authors have read and agreed to the published version of the manuscript.

Funding: This research received no external funding.

Institutional Review Board Statement: Not applicable.

Informed Consent Statement: Not applicable.

Data Availability Statement: Not applicable.

Conflicts of Interest: The authors declare no conflict of interest.

References

1. Styla, S.A. New Grinding Technology Using an Electromagnetic Mill—Testing the Efficiency of the Process. *ECONTECHMOD Int. Q. J. Econ. Technol. Model. Process.* **2017**, *6*, 81–88.
2. Wolosiewicz-Glab, M.; Pieta, P.; Foszcz, D.; Ogonowski, S.; Niedoba, T. Grinding Kinetics Adjustment of Copper Ore Grinding in an Innovative Electromagnetic Mill. *Appl. Sci.* **2018**, *8*, 1322. [[CrossRef](#)]
3. Ogonowski, S.; Ogonowski, Z.; Swierzy, M. Power optimizing control of grinding process in electromagnetic mill. In Proceedings of the 21st International Conference on Process Control (PC), Strbske Pleso, Slovakia, 6–9 June 2017; pp. 370–375. [[CrossRef](#)]
4. Volkov, V.S.; Bezzubceva, M.M.; Zagajevski, N.N. K Voprosu proektirovaniya diskovikh elektromagnitnikh mekhanoaktivatorov v apparaturno-tehnologicheskikh sistemakh proizvodstva kormovikh dobavok. *Sovrem. Nauk. Tekhnologii* **2015**, 11–13.
5. Styla, S. Laboratory studies of an electromagnetic mill inductor with a power source. *ECONTECHMOD Int. Q. J. Econ. Technol. Model. Process.* **2017**, *6*, 109–114.
6. Wolosiewicz-Glab, M.; Foszcz, D.; Ogonowski, S. Design of the electromagnetic mill and the air stream ratio model. *IFAC-Pap. OnLine* **2017**, *50*, 14964–14969. [[CrossRef](#)]
7. Wolosiewicz-Glab, M.; Pieta, P.; Niedoba, T.; Foszcz, D. Approximation of Partition Curves for Electromagnetic Mill with Inertial Classifier—Case study. In *IOP Conference Series: Earth and Environmental Science*; IOP Publishing: Bristol, UK, 2017; Volume 95, p. 042037. [[CrossRef](#)]
8. Wolosiewicz-Glab, M.; Ogonowski, S.; Foszcz, D.; Gawenda, T. Assessment of classification with variable air flow for inertial classifier in dry grinding circuit with electromagnetic mill using partition curves. *Physicochem. Probl. Miner. Process* **2018**, *54*, 440–447. [[CrossRef](#)]
9. Garg, A.; Lam, J.S.L.; Gao, L. Energy conservation in manufacturing operations: Modelling the milling process by a new complexity-based evolutionary approach. *J. Clean. Prod.* **2015**, *108*, 34–45. [[CrossRef](#)]
10. Krawczykowski, D.; Foszcz, D.; Ogonowski, S.; Gawenda, T.; Wolosiewicz-Glab, M. Analysis of the working chamber size influence on the effectiveness of grinding in electromagnetic mill. In *IOP Conference Series: Materials Science and Engineering*; IOP Publishing: Bristol, UK, 2018; Volume 427, p. 012033. [[CrossRef](#)]
11. Bazin, C.; St-Pierre, M.; Hodouin, D. Calibration of the perfect mixing model to a dry grinding mill. *Powder Technol.* **2005**, *149*, 93–105. [[CrossRef](#)]
12. Całus, D.; Makarchuk, O. Analysis of interaction of forces of working elements in electromagnetic mill. *Prz. Elektrotechniczny* **2019**, *12*, 64–69. [[CrossRef](#)]
13. Makarchuk, O.; Calus, D.; Moroz, V. Mathematical model to calculate the trajectories of electromagnetic mill operating elements. *Tech. Electrodyn.* **2021**, *2*, 26–34. [[CrossRef](#)]
14. Makarchuk, O.; Calus, D. Research of the performance indicator of an electromagnetic mill. *Tech. Electrodyn.* **2022**, *1*, 50–57. [[CrossRef](#)]
15. Całus, D. Analysis of the Thermal Processes in an Electromagnetic Mill. *Energies* **2022**, *15*, 7899. [[CrossRef](#)]
16. Ostrowski, M.; Błachowski, B.; Bocheński, M.; Piernikarski, D.; Filipek, P.; Janicki, W. Design of nonlinear electromagnetic energy harvester equipped with mechanical amplifier and spring bumpers. *Bull. Pol. Acad. Sci. Tech. Sci.* **2020**, *68*, 1373–1383. [[CrossRef](#)]
17. Ogonowski, S.; Ogonowski, Z.; Pawelczyk, M. Multi-objective and multi-rate control of the grinding and classification circuit with electromagnetic mill. *Appl. Sci.* **2018**, *8*, 506. [[CrossRef](#)]
18. Ogonowski, S.; Bismor, D.; Ogonowski, Z. Control of complex dynamic nonlinear loading process for electromagnetic mill. *Arch. Control. Sci.* **2020**, *30*, 471–500. [[CrossRef](#)]
19. Ogonowski, S. On-Line Optimization of Energy Consumption in Electromagnetic Mill Installation. *Energies* **2021**, *14*, 2380. [[CrossRef](#)]
20. Buchczik, D.; Wegehaupt, J.; Krauze, O. Indirect measurements of milling product quality in the classification system of electromagnetic mill. In Proceedings of the 22nd International Conference Methods and Models in Automation and Robotics (MMAR), Międzyzdroje, Poland, 28–31 August 2017; pp. 1039–1044. [[CrossRef](#)]
21. Wegehaupt, J.; Buchczik, D.; Krauze, O. Preliminary studies on modelling the drying process in product classification and separation path in an electromagnetic mill installation. In Proceedings of the 22nd International Conference on Methods and Models in Automation and Robotics (MMAR), Międzyzdroje, Poland, 28–31 August 2017; pp. 849–854. [[CrossRef](#)]

22. Budzan, S. Automated grain extraction and classification by combining improved region growing segmentation and shape descriptors in electromagnetic mill classification system. In Proceedings of the Tenth International Conference on Machine Vision (ICMV 2017), Vienna, Austria, 13–15 November 2017; p. 106960B. [[CrossRef](#)]
23. Szczepaniak, K.; Skorupska, B.; Kubacz, N. Research on the grinding process of copper semi-finished products in an electromagnetic mill. *Cuprum Czas. Nauk. Tech. Górnictwa Rud* **2015**, *2*, 47–53.
24. Styła, S. Examination of an electromagnetic mill structure by means of infrared radiation. *Przegląd Elektrotechniczny* **2014**, *90*, 179–182. [[CrossRef](#)]
25. Ogonowski, S.; Wolosiewicz-Glab, M.; Ogonowski, Z.; Foszcz, D.; Pawelczyk, M. Comparison of wet and dry grinding in electromagnetic mill. *Minerals* **2018**, *8*, 138. [[CrossRef](#)]
26. Ruslan, I.; Evgenij, K.; Ludmila, P.; Timur, D.; Azat, K. The Influence of Physical Activation of Portland Cement in the Electromagnetic Vortex Layer on the Structure Formation of Cement Stone: The Effect of Extended Storage Period and Carbon Nanotubes Modification. *Buildings* **2022**, *12*, 711. [[CrossRef](#)]
27. Sławiński, K.; Knaś, K.; Gandor, M.; Balt, B.; Nowak, W. Electromagnetic mill and its application for coal grinding and drying. *Piece Przemysłowe Kotły* **2014**, *1–2*, 21–25.
28. Khaydarov, B.; Suvorov, D.; Pazniak, A.; Kolesnikov, E.; Gorchakov, V.; Mamulat, S.; Kuznetsov, D. Efficient method of producing clinker-free binding materials using electromagnetic vortex milling. *Mater. Lett.* **2018**, *226*, 13–18. [[CrossRef](#)]
29. Gandor, M.; Sławiński, K.; Knaś, K.; Balt, B.; Nowak, W. Application of inverse analysis in electromagnetic grinding of brown coal to obtain an optimal particle size distribution—a heuristic approach. *Comput. Assist. Methods Eng. Sci.* **2014**, *21*, 187–197.
30. ANSYS, Inc. Theory Reference. In *ANSYS Release 9.0. 002114*; SAS IP Inc.: Cheyenne, WY, USA, 2004; 1067p.
31. Benson, D.J.; Hallquist, J.O. A simple rigid body algorithm for structural dynamics programs. *Int. J. Numer. Methods Eng.* **1986**, *22*, 723–749. [[CrossRef](#)]
32. LS-DYNA®. Theory Manual, Livermore Software Technology Corporation. 2006. 680p. Available online: https://www.egr.msu.edu/decs/sites/default/files/content/ls-dyna_theory_manual_2006.pdf (accessed on 7 August 2022).
33. Hughes, T.J.R.; Taylor, R.L.; Sackman, J.L.; Curnier, A.C.; Kanoknukulchai, W. A Finite Element Method for a Class of Contact-Impact Problems. *J. Comp. Meths. Appl. Mechs. Eng.* **1976**, *8*, 249–276. [[CrossRef](#)]
34. Brown, D.; Christian, W.; Hanson, R. Tracker Video Analysis and Modeling Tool, Copyright (c). 2021. Available online: <https://physlets.org/tracker/> (accessed on 7 August 2022).

Disclaimer/Publisher’s Note: The statements, opinions and data contained in all publications are solely those of the individual author(s) and contributor(s) and not of MDPI and/or the editor(s). MDPI and/or the editor(s) disclaim responsibility for any injury to people or property resulting from any ideas, methods, instructions or products referred to in the content.